AIAA SciTech Forum
January 3-7, 2022, San Diego, CA & Virtual
AIAA SCITECH 2022 Forum
10.2514/6.2022-1160

Spin Aerodynamic Modeling for a Fixed-Wing Aircraft Using Flight Data

James L. Gresham*, Benjamin M. Simmons†, Jeremy W. Hopwood‡, and Craig A. Woolsey§
Virginia Tech, Blacksburg, Virginia 24061

Novel techniques are used to identify a nonlinear, quasi-steady, coupled, spin aerodynamic model for a fixed-wing aircraft from flight test data. Orthogonal phase-optimized multisine inputs are used as excitation signals while collecting spinning flight data. A novel vector decomposition of explanatory variables leads to an elegant model structure for spin flight data analysis. Results shows good agreement with validation flight data. This effort was motivated by interest in developing a flight termination system for a fixed-wing unmanned aircraft that controls a descending spiral trajectory toward a designated impact area. The design and tuning of the control law, which is described in a separate paper, benefits from a model of the aircraft dynamics and control authority in the neighborhood of a stable, oscillatory spin.

Nomenclature

a_x, a_y, a_z	=	body-axis translational acceleration, ft/s^2 or g
b	=	projected wingspan, ft
$\bar{c}$	=	mean aerodynamic chord, ft
C_l, C_m, C_n	=	body-axis aerodynamic moment coefficients
C_x, C_y, C_z	=	body-axis aerodynamic force coefficients
g	=	gravitational acceleration, ft/s^2
I_{xx}, I_{yy}, I_{zz}	=	moments of inertia, slug-ft^2
I_{xy}, I_{xz}, I_{yz}	=	products of inertia, slug-ft^2
$\mathcal{L}, \mathcal{M}, \mathcal{N}$	=	body-axis aerodynamic moments, ft-lbf
m	=	aircraft mass, slug
p, q, r	=	body-axis angular velocity components, rad/s or deg/s
$\bar{q} = \frac{1}{2}\rho {V_t}^2$	=	dynamic pressure, lbf/ft^2
S	=	projected wing area, ft^2
T	=	thrust, lbf
u, v, w	=	body-axis translational velocity components, ft/s
V_t	=	true airspeed, ft/s
X, Y, Z	=	body-axis aerodynamic forces, lbf
α	=	angle of attack, rad or deg
β	=	angle of sideslip, rad or deg
$\delta_a, \delta_e, \delta_r$	=	control surface deflections, rad or deg
ϕ, θ, ψ	=	inertial orientation Euler angles, rad or deg
ρ	=	air density, slug/ft^3
σ	=	parameter estimate uncertainty bound
$\hat{\theta}$	=	parameter estimate

*Graduate Student, Crofton Department of Aerospace and Ocean Engineering, Senior Member AIAA. jamesgresham@vt.edu
†Graduate Student, Crofton Department of Aerospace and Ocean Engineering, Member AIAA. bsimm11@vt.edu
‡Graduate Student, Crofton Department of Aerospace and Ocean Engineering, Student Member AIAA. jeremyhopwood@vt.edu
§Professor, Crofton Department of Aerospace and Ocean Engineering, Associate Fellow AIAA. cwoolsey@vt.edu

I. Introduction

System identification of an aerodynamic model for stall and spin conditions is typically accomplished from data collected in a wind tunnel or using computational fluid dynamics. This study presents the methodology and results of identifying a nonlinear, quasi-steady, coupled, aerodynamic model for a fixed-wing unmanned aircraft in a spinning descent from flight test data. The need for such a model arises in scenarios where one wishes to influence the helical trajectory through control, such as in Ref. [1]. A flight test experiment was designed and conducted using automated orthogonal phase-optimized multisine inputs [2, 3] for excitation while in a stable spin. Time-domain techniques were used with equation error methods to develop the model structure and to estimate parameter values for both nominal and spinning flight. The developed aerodynamic models were then validated using independent flight test data.

Many modern unmanned aerial vehicles (UAVs), including the RQ-4 Global Hawk, are equipped with a flight termination sequence used in the event of an in-flight emergency, such as loss of propulsion or communication [4]. One common flight termination approach is to put the aircraft in an intentional spin, thereby giving a steady descent with a small impact radius and a relatively low impact speed as compared to a gliding or spiral descent. A spin descent's main advantage is dissipation of energy in a stable, predictable, and controlled manner [5]. One major reason a vertical stall spin is an effective failsafe is that it is typically a stable, steady-state-periodic trajectory for fixed aileron, elevator, and rudder deflections. Some control authority is maintained in this state of motion, since this authority was required to establish the motion in the first place, and thus it may be desirable to direct the spinning descent along a prescribed path to impact within a "safe" crash zone, as discussed in Refs. [6, 7]. To aid development of a robust, model-based control law that directs the spinning descent of an aircraft along a desired azimuth and inclination angle [1], an aerodynamic model is needed that adequately describes aircraft motion in a neighborhood of the steady spin.

The primary new contribution of this work is a methodology for developing a nonlinear, quasi-steady, coupled, aerodynamic model for a fixed-wing unmanned aircraft in a spinning descent. This system identification methodology includes, to the best of the authors' knowledge, the first use of multisine inputs as excitation signals while collecting spinning flight data and a novel decomposition of explanatory variables which leads to an elegant model structure to adequately describe spin dynamics using flight data. This paper uses techniques developed in Refs. [8, 9] and theory and processes developed in concurrent efforts [1, 10]. Ref. [1], in particular, describes the development of parallel linear quadratic and robust H_∞ controllers that can adjust the direction of a spinning descent to improve predictability and safety during an intentional flight termination. A separate effort will compare results of that controller tuned with the nominal glide model and the spin model presented here.

Prior research efforts on aircraft spin modeling were studied to gain insight into the current state of spin modeling theory, excitation techniques, analysis methods, and best practices. Fixed-wing aircraft spin behavior was studied intensively by the National Aeronautics and Space Administration (NASA) in the 1980s, with the primary aim of spin prevention and spin recovery in piloted aircraft. These studies were focused on spin characteristics and primarily based on rotary balance wind tunnel data [11, 12]. Subsequent NASA research blended vertical spin tunnel data with forced oscillation wind tunnel data to model aircraft spin dynamics [13]. Ref. [14] studied the uncertainty of spin aerodynamic model parameter estimates using these blending techniques for a large database of wind tunnel experiments. Ref. [15] demonstrated the importance of modeling unsteady effects for stall-spin departure dynamics. Refs. [16, 17] describe the NASA 20-Foot Vertical Spin Tunnel and test methods for spin susceptibility, spin recovery, and stable spin characterization. Similar to this paper, Refs. [18, 19] each developed a nonlinear aerodynamic model for spinning flight using flight test data alone. Ref. [18] used local model networks partitioned based on the angle-of-attack and highlighted the importance of kinematic consistency of measured states for spin flight data. Ref. [19] combined two novel modeling methods: the ensemble empirical mode decomposition technique and the extended multipoint modeling approach. In contrast with the present paper, Refs. [18, 19] did not excite the aircraft dynamics with control surface perturbations once in a stall spin. Ref. [19] also incorporated numerous nonlinear model terms relative to the quantity of modeling flight data, raising the possibility of an overfit model.

This paper addresses a particular need for technical guidance concerning flight testing and data analysis for the identification of a flight dynamic model that adequately describes the response of a fixed-wing aircraft to control and other perturbations from a stable, oscillatory spinning motion. The remainder of the paper is organized as follows. Section II briefly describes stable, steady spinning flight and the modeling process. Section III describes the aircraft flown in this effort and design of the flight test experiments. Section IV presents results from flight tests and system identification. Section V discusses conclusions, as well as plans for ongoing work.

II. Background

A. Aerodynamics of a Spin

The spin condition for a fixed-wing aircraft in classical aviation is a rotating stall which is "driven by adverse yaw and post-stall lift differences" [20]. Aircraft with ailerons, as opposed to spoilers, experience adverse yaw from differential drag-due-to-lift which creates a yawing moment away from the direction of a roll input. If large aileron inputs are applied near the stall angle-of-attack, without sufficient rudder to counteract the adverse yaw, an aircraft can enter a spin. This spin may progress to a stable spin without proper inputs to reduce the angle-of-attack below stall [20]. A spin may also be intentionally entered by approaching the stall angle-of-attack and then, at the onset of stall, applying large rudder inputs in the desired spin direction. Subsequent aileron inputs might reinforce the spin, or counteract the steady spin. A spin is described by four phases: spin entry, incipient spin, steady (or developed) spin, and spin recovery [21]. The pilot techniques necessary for spin entry and spin recovery were necessary for this flight test effort; however, the focus of this paper is on modeling and predicting aircraft dynamic response in the steady spin phase.

A classic stable spin is characterized by steady motion with constant angle-of-attack (α), angle-of-sideslip (β), spin rate (Ω), and descent rate while the aircraft follows a vertical helical path. An oscillatory spin has a similar vertical helical path; however, α and β oscillate about their respective average values. The aircraft studied in this effort has a stable oscillatory spin as shown later in Fig. 4b.

B. Dynamic Modeling of a Spin

A fixed-wing aircraft's aerodynamic response to small perturbations from steady, level flight at a low angle-of-attack is well characterized by a linear flight dynamic model, $f(\alpha, \beta, p, q, r, \delta_e, \delta_a, \delta_r)$, where the equations of motion decouple into longitudinal and lateral-directional components. Aggressive, out-of-plane flight maneuvers such as a stall spin are best described by a nonlinear flight dynamic model where the equations of motion are fully coupled due to aerodynamic and rotating reference frame effects. This is also true when describing dynamic perturbations from a given steady motion outside of the pre-stall envelope, such as while in a stable spin.

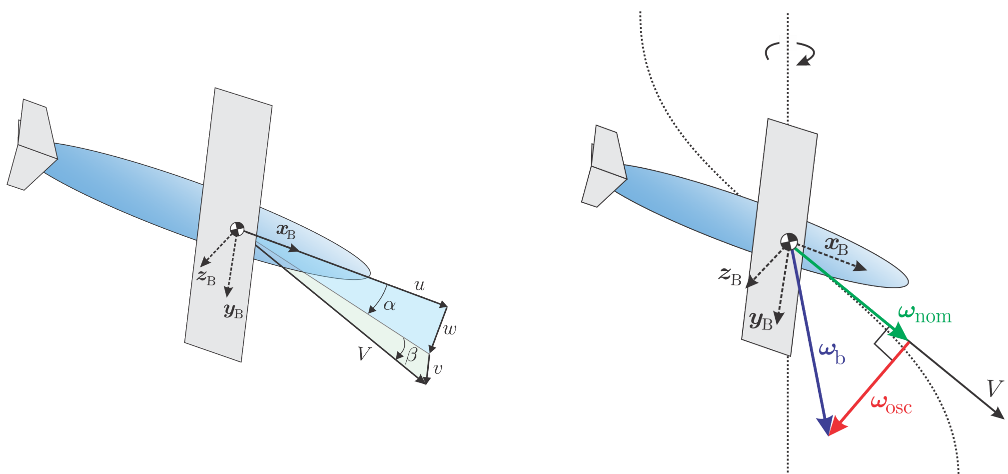

Fig. 1 Spin dynamic motion notation.

With inspiration from Refs. [11–13], the flight data recorded on-board the aircraft are transformed into states better suited to characterizing spinning motion. The body-axis angular velocity (ω_b) is decomposed, as depicted in Fig. 1, into components along (ω_{nom}) and orthogonal to (ω_{osc}) the flight path:

$$\omega_b = \begin{bmatrix} p \\ q \\ r \end{bmatrix}, \quad \omega_{nom} = \begin{bmatrix} \Omega \\ 0 \\ 0 \end{bmatrix}, \quad \omega_{osc} = \begin{bmatrix} p_{osc} \\ q_{osc} \\ r_{osc} \end{bmatrix} \tag{1}$$

In this notation, ω_{nom} is the projection of ω_b onto the instantaneous wind vector. Because the body-axis angular velocity vector and wind vector share an origin at the center of gravity, ω_{nom} has only a single component which is the angular rate about the wind vector, denoted Ω. The orthogonal complement, ω_{osc}, comprises three rates which are denoted as the body-axis oscillatory components as they describe residual body-axis oscillations that are not directly about the instantaneous wind vector. For a nominal stall spin with no oscillations or excitations, Ω in Eq. (1) is the classical spin rate and $\omega_{\text{osc}} = \mathbf{0}$. This notation is relatively consistent with that used for blending vertical spin tunnel rates and forced oscillation rates from wind tunnel data [13, 22]. The rate components are calculated from

$$\Omega = p\cos\alpha\cos\beta + q\sin\beta + r\sin\alpha\cos\beta \tag{2}$$

$$p_{\text{osc}} = p - \Omega\cos\alpha\cos\beta \tag{3}$$

$$q_{\text{osc}} = q - \Omega\sin\beta \tag{4}$$

$$r_{\text{osc}} = r - \Omega\sin\alpha\cos\beta \tag{5}$$

The measured body-axis angular rates decomposed to the wind vector and the residual oscillatory components are used during the model structure determination phase of system identification. This transformation, based on aerodynamic spin theory, resulted in significantly improved modeling results.

C. Aircraft System Identification

System identification is the process of developing a mathematical model of a physical system based on observed data from the system [23]. The objective of system identification is to create a *useful* system model based on measured or calculated *outputs* and *inputs*. The system identification process is composed of multiple steps which typically result in a set of differential or algebraic equations describing system behavior. Aircraft system identification seeks to develop an aerodynamic model that adequately describes the aircraft motion or response (outputs) to controls or perturbations (inputs). System identification is performed using imperfect knowledge of the inputs and outputs due to sensor noise, process noise, sensor scale factors, and bias that must be accounted for during analysis. The aircraft system identification methodology, inspired by Ref. [2], and adapted for the small, fixed-wing UAV research in Refs. [8, 9], is shown in Fig. 2.

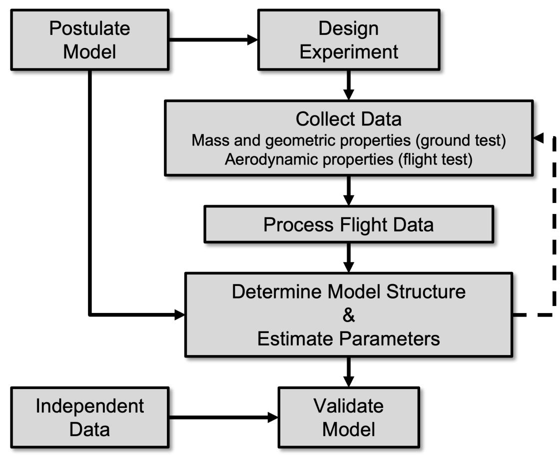

Fig. 2 Aircraft system identification process for a small fixed-wing aircraft (adapted from Ref. [2]).

For this work, data compatibility, or kinematic consistency, analysis was accomplished using both integration and smoothed differentiation of kinematic states and measurements. Next, the model structure was determined from experimental data using multivariate orthogonal function (MOF) modeling [2, 24]. Values for the unknown model parameters were determined using the equation-error method [2, 25]. Finally, the model was validated using flight data which were not used in the modeling process.

System identification from flight data requires low pairwise correlation between individual explanatory variables in order to identify each variable's contribution to the aircraft dynamic response. One excitation technique used in system identification research is the orthogonal phase-optimized multisine input [2, 3]. Orthogonal multisine inputs were developed and applied to multiple control surfaces to excite aircraft motion about all three axes concurrently. This technique offers the primary advantage of providing sufficiently rich excitation while minimizing test time. The technique ensures low correlation between the control inputs which improves the modeling results. Design of multisine inputs does not require *a priori* information of the aircraft dynamics, but it does require precisely scripted, automated control inputs [26]. The efficient excitation offered by multisine inputs is well suited to the short duration stall spin maneuvers performed in this research.

D. Aerodynamic Model Structure

A model framework is initially postulated from physical principles to aid in designing the experiment, and then the final aerodynamic model structure is determined based on aerodynamic phenomena reflected in experimental data. The model framework takes the form of the rigid body equations of motion (EOM). The aircraft was modeled as a rigid body of mass m with known principle moments of inertia I_{xx}, I_{yy}, and I_{zz}, and product of inertia I_{xz}. The remaining products of inertia, I_{xy} and I_{yz}, were assumed to be zero based on lateral symmetry.

The 6 degree-of-freedom (6-DOF) body-axis EOM are

Rotational kinematic equations

$$p = -\dot{\psi}\sin\theta + \dot{\phi} \tag{6}$$
$$q = \dot{\psi}\sin\phi\cos\theta + \dot{\theta}\cos\phi \tag{7}$$
$$r = \dot{\psi}\cos\phi\cos\theta - \dot{\theta}\sin\phi \tag{8}$$

Translational dynamics (force) equations

$$X = m(\dot{u} - rv + qw + g\sin\theta) \tag{9}$$
$$Y = m(\dot{v} + ru - pw - g\sin\phi\cos\theta) \tag{10}$$
$$Z = m(\dot{w} - qu + pv - g\cos\phi\cos\theta) \tag{11}$$

Rotational dynamics (moment) equations

$$\mathcal{L} = \dot{p}I_{xx} + qr(I_{zz} - I_{yy}) - (\dot{r} + pq)I_{xz} \tag{12}$$
$$\mathcal{M} = \dot{q}I_{yy} - pr(I_{zz} - I_{xx}) + (p^2 - r^2)I_{xz} \tag{13}$$
$$\mathcal{N} = \dot{r}I_{zz} + pq(I_{yy} - I_{xx}) + (qr - \dot{p})I_{xz} \tag{14}$$

The aerodynamic forces (X, Y, Z) and moments $(\mathcal{L}, \mathcal{M}, \mathcal{N})$ are expressed in the non-dimensional form

$$C_x = \frac{X}{\bar{q}S}, \quad C_y = \frac{Y}{\bar{q}S}, \quad C_z = \frac{Z}{\bar{q}S} \tag{15}$$

$$C_l = \frac{\mathcal{L}}{\bar{q}Sb}, \quad C_m = \frac{\mathcal{M}}{\bar{q}S\bar{c}}, \quad C_n = \frac{\mathcal{N}}{\bar{q}Sb} \tag{16}$$

to remove dependence on dynamic pressure ($\bar{q} = \rho {V_t}^2/2$) and aircraft size.

Aircraft system identification is accomplished by obtaining expressions for the aerodynamic force and moment coefficients [2, 25]. Aerodynamic force coefficients are estimated using mass (m), dynamic pressure ($\bar{q}$), body-frame measurements of translational acceleration (a_x, a_y, a_z), and thrust (T) which is assumed here to act along the body x-axis:

$$C_x = \frac{ma_x - T}{\bar{q}S} \tag{17}$$
$$C_y = \frac{ma_y}{\bar{q}S} \tag{18}$$
$$C_z = \frac{ma_z}{\bar{q}S} \tag{19}$$

This research involved maneuvers with idle propulsion; thus, the separate thrust model is omitted and windmilling propeller effects are included directly into the aerodynamic model. The aerodynamic moment coefficients are calculated by combining the non-dimensional moment equations shown in Eq. (16) and the rotational dynamics equations, Eqs. (12)-(14), leading to

$$C_l = \frac{1}{\bar{q}bS}\left(I_{xx}\dot{p} - I_{xz}\left(\dot{r} + pq\right) + qr\left(I_{zz} - I_{yy}\right)\right) \tag{20}$$

$$C_m = \frac{1}{\bar{q}\bar{c}S}\left(I_{yy}\dot{q} + rp\left(I_{xx} - I_{zz}\right) + I_{xz}\left(p^2 - r^2\right)\right) \tag{21}$$

$$C_n = \frac{1}{\bar{q}bS}\left(I_{zz}\dot{r} - I_{xz}\left(\dot{p} - qr\right) + pq\left(I_{yy} - I_{xx}\right)\right) \tag{22}$$

Direct measurements of angular acceleration are unavailable, so these terms are obtained as smoothed derivatives of the angular rate measurements [2].

III. Flight Test Experiments

A. Research Aircraft and Instrumentation

The radio-controlled (RC), fixed-wing aircraft selected for testing was the E-flite Carbon-Z Cessna 150 (CZ150), shown in Fig. 3. The aircraft is electrically powered by a six-cell 22.2V 5000mAh lithium-polymer battery, with a tractor propeller configuration using a single 16-in. diameter, 8-in. pitch (16x8) Aeronaut CamCarbon folding propeller. The CZ150 aircraft was instrumented with a Pixhawk flight computer for data collection, specifically a Pixhawk CubePilot Cube Orange flight controller running PX4 firmware [27]. Additionally, an on-board co-computer was used for automated input generation and subsequent control law implementation. The co-computer was a Raspberry Pi 4 running Ubuntu Linux distribution, communicating with the Pixhawk using Mavlink protocols, and utilizing the Robot Operating System (ROS) libraries. The Pixhawk sensor suite includes an attitude and heading reference system (AHRS), a pitot-static probe, and a real-time kinematic (RTK) global positioning system (GPS) receiver. Details concerning post-flight data processing and co-computer inputs are presented in Ref. [10].

Fig. 3 CZ150 fixed-wing research aircraft.

Table 1 The CZ150 mass and geometric properties

Property	Symbol	Value	Units
Mass	m	0.336	slug
Mean aerodynamic chord	$\bar{c}$	1.049	ft
Projected wing span	b	6.97	ft
Projected wing area	S	7.31	ft^2
Roll moment of inertia	I_{xx}	0.457	slug-ft^2
Pitch moment of inertia	I_{yy}	0.357	slug-ft^2
Yaw moment of inertia	I_{zz}	0.622	slug-ft^2
Product of inertia	I_{xz}	0.052	slug-ft^2
Products of inertia	I_{xy}, I_{yz}	~0	slug-ft^2

The CZ150 was chosen primarily for its ability to enter and maintain a spin, as well as benign spin recovery characteristics. Additional advantages are its simple construction, satisfactory handling qualities, and sufficient payload to incorporate the desired instrumentation package and on-board co-computer. The CZ150 mass and geometric properties, tabulated in Table 1, were determined with methods described in Ref. [8]. The principle moments of inertia (MoI) were measured experimentally using the compound pendulum technique [28] and the product of inertia I_{xz} was determined using a test described in Ref. [2]. The remaining products of inertia, I_{xy} and I_{yz}, were assumed to be zero based on lateral symmetry.

The Pixhawk PX4 firmware includes an extended Kalman filter (EKF) state estimator that provides orientation angles and earth-fixed velocity [29]. The pulse-width modulation (PWM) signal sent from the Pixhawk to each control surface servo was used to determine control surface deflection angle based on a servo-actuator model. The aircraft instrumentation system lacked air data angle sensors; therefore, α and β were derived from the EKF states. While the authors were originally skeptical of this approach in a stall spin, kinematic consistency analysis in Sec. IV shows the derived values of α and β are suitable for use even in this flight regime. Data processing makes use of work by the second author [9, 30] with refinements described in Ref. [10].

B. Experiment Design

Flight test data collection was accomplished over a series of flights at the Kentland Experimental Aerial Systems (KEAS) Laboratory located at Virginia Tech's Kentland Farm agricultural research facility [31].

The nominal glide model was developed from a collection of 8 nominal gliding maneuvers with multisine excitations active on each control surface. Each maneuver included 1 second of trimmed flight followed by 30 seconds of excitation. The spin model was developed from a collection of 18 spin maneuvers with multisine excitations active on each control surface. For each spin maneuver, the pilot progressed through a series of scripted test inputs:

1) Initiate benign, wings-level, power-off stall (δ_e: 70% trailing-edge up gradually, δ_a,δ_r: as reqd. to level wings)
2) At stall break, initiate spin inputs (δ_r: 70% left, δ_e: maintain 70% trailing-edge up, δ_a: 50% left)
3) After two spin rotations, initiate multisine excitation

4) At predetermined safe recovery altitude, terminate the multisine excitation and recover to resume normal flight

The precise control surface deflections were obtained during test maneuvers by modifying the RC limits in flight with pilot adjustment of a transmitter switch, thus allowing the pilot to maintain a precise spin by holding the maximum control inputs on the RC transmitter. Each spin maneuver used for system identification included only the data involving multisine excitation, after development of a steady spin. The useful data record was typically 7 to 12 seconds in length, depending on the initial and final altitudes. The short maneuver length and irregularities in the data due to the nonlinear flight regime made more maneuvers desirable for spin modeling.

C. Stable Oscillatory Spin

During each flight executed to collect spin modeling data, a nominal spin without excitation inputs was accomplished to demonstrate repeatability of the steady spinning motion and of the four spin phases, including benign spin recovery characteristics. The flight path from one experimental flight test maneuver is shown in Fig. 4a, illustrating entry and initial development of the incipient spin, the fully developed steady spinning motion, and a successful recovery. The aircraft orientation is shown at a 10 Hz interval with the flight path displayed based on the data recorded at 50 Hz. An

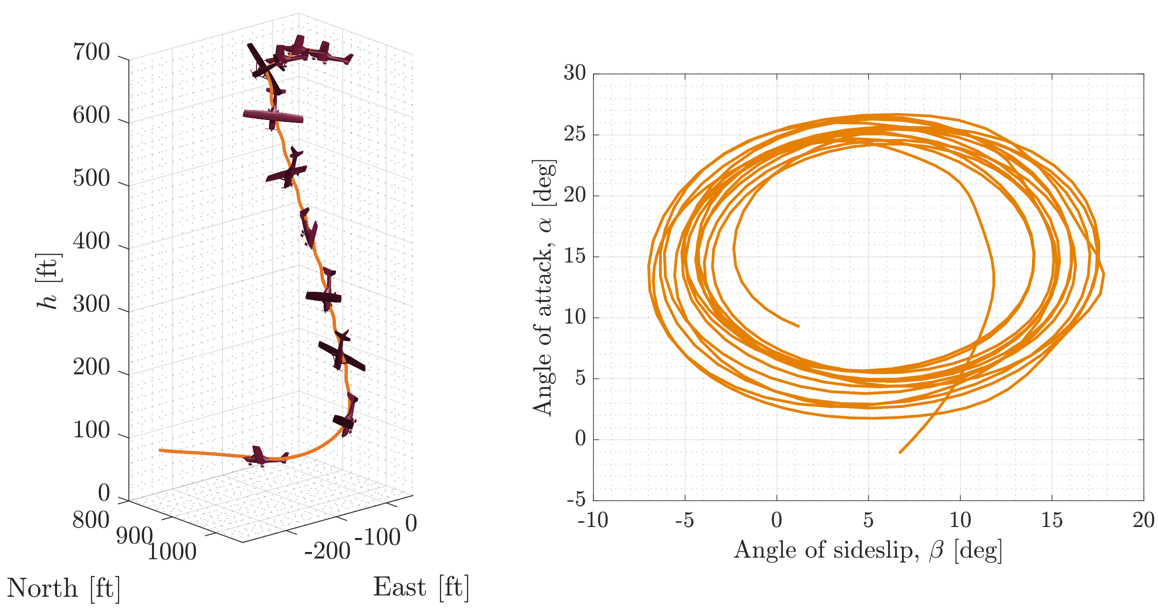

(a) Flight path showing spin phases

(b) α-β trace showing stable oscillatory spin

Fig. 4 Experimental flight data from a nominal spin maneuver.

α-β trace from the maneuver is shown in Fig. 4b with the oscillatory spin clearly evident, as discussed in Sec. II.A. The aerodynamic spin model developed is valid around a perturbation range from this nominal spin. Nominal spin data were collected with 70% left rudder deflection, 70% trailing-edge up elevator, and 50% aileron deflection for left roll input. These inputs were selected to ensure the controls were not saturated with the multisine inputs active and the aircraft remained in a stall spin during multisine excitation. The selected nominal control inputs permit actuator deflections in the follow-on effort [1] to control the descent path while maintaining a spin. Steady nominal spin state and control input values determined from flight data are

$$\begin{array}{llll} & \tilde{V}_t = 66.9 \text{ ft/s} & \tilde{p} = -385 \text{ deg/s} & \tilde{\delta}_a = 15.5 \text{ deg} \\ \tilde{\phi} = -24.0 \text{ deg} & \tilde{\alpha} = 12.4 \text{ deg} & \tilde{q} = 36.2 \text{ deg/s} & \tilde{\delta}_e = -18.5 \text{ deg} \\ \tilde{\theta} = -74.0 \text{ deg} & \tilde{\beta} = 5.74 \text{ deg} & \tilde{r} = -97.2 \text{ deg/s} & \tilde{\delta}_r = 24.6 \text{ deg} \end{array} \tag{23}$$

where $\tilde{\cdot}$ denotes the nominal spin quantity.

IV. Results

The aircraft system identification methodology presented in Sec. II.C was followed to produce a nonlinear, coupled aerodynamic model in both a nominal glide and a steady spin. The models were developed using only flight test data without excessive disturbances, data dropouts, or poor kinematic consistency. Modeling was performed using flight data with multisine inputs enabled in a nominal glide and a stable spin, and using the techniques and processing tools discussed in Sec. II. Validation was accomplished using data from independently designed multisine input maneuvers. Data analysis was conducted in MATLAB® [32] with use of analytic tools developed by the authors and those provided in System IDentification Program for AirCraft (SIDPAC) [2].

A. Data Compatibility

Figure 5 shows a data compatibility analysis plot for a spin maneuver with multisine excitation. The figure shows corrected data used for system identification analysis, raw data obtained from the instrumentation system, and flight path reconstruction (FPR) signals calculated from other measurements to confirm validity of the kinematic consistency corrections. The reconstructed measurements and data processing, including smoothing and correction for sensor bias, were accomplished as discussed in Ref. [10]. After correction, the measured and reconstructed signals agree well, showing that the data have been sufficiently conditioned to proceed with system identification. Most notably, the derived α and β data obtained from the stalled oscillatory spin agree well with the reconstructed signals.

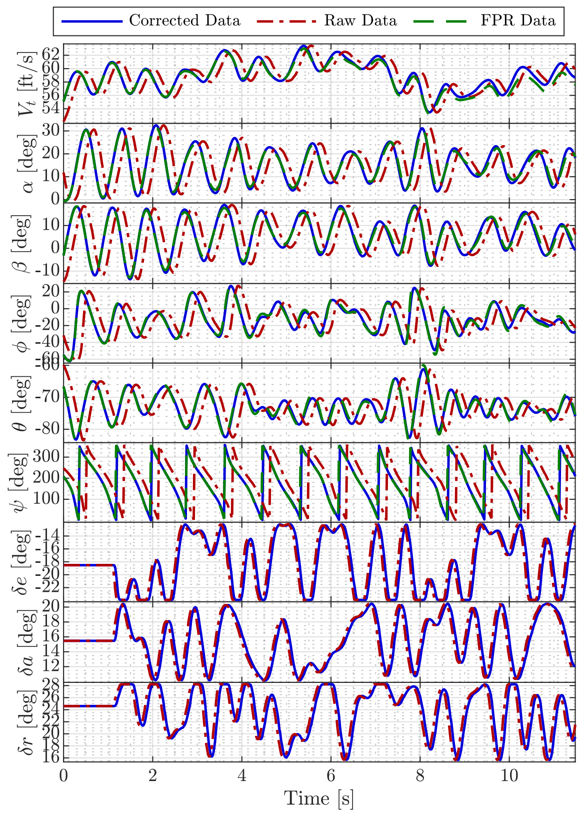

Fig. 5 Data compatibility for spin, multisine inputs.

B. Model Structure

For this research, MOF modeling [2, 24] was employed for initial model structure determination and then analyst insight used to refine the model structure. The cutoff for modeling terms was determined automatically using both predicted squared error (PSE) and coefficient of determination (R^2) values following rules of thumb presented in Ref. [33].

The explanatory variables used to represent the aerodynamic force and moment coefficients for the nominal glide in this research were α, β, the non-dimensional body-axis angular rate components

$$\hat{p} = \frac{pb}{2V_t}, \quad \hat{q} = \frac{q\bar{c}}{2V_t}, \quad \hat{r} = \frac{rb}{2V_t},$$

and the control surface angular deflections δ_e, δ_a, and δ_r. This model structure facilitated convenient control law tuning, and the nominal glide model developed with these explanatory variables produced good matching with validation data; no additional explanatory variables were considered.

Initially, the same explanatory variables were used for spin modeling; however, this provided an insufficient model structure to describe the spin dynamics. Drawing inspiration from Refs. [11–13], and as described in Sec. II, the body-axis recorded rates were transformed to the wind-axis angular rate (Ω) and the complementary body-axis oscillatory components (p_{osc}, q_{osc}, and r_{osc}) using Eqs. (2)-(5). Furthermore, based on demonstrated spin model improvement by including unsteady effects in Ref. [15], the quasi-steady terms $\dot{\alpha}$ and $\dot{\beta}$ were considered; this significantly improved the dynamic model's predictive performance. States used in previous wind tunnel modeling efforts were also considered, including wing tilt angle, spin helix angle, and spin radius. While these states are simple to determine for wind tunnel tests, where the test setup is highly structured and the spinning motion is correspondingly constrained, they are difficult to accurately determine for an aircraft in flight. Thus, the explanatory variables used to represent the aerodynamic force and moment coefficients for spinning motion were limited to α, β, their nondimensional quasi-steady rates

$$\hat{\alpha} = \frac{\dot{\alpha}\,\bar{c}}{2V_t}, \quad \hat{\beta} = \frac{\dot{\beta}\,b}{2V_t},$$

the non-dimensional spin angular rates

$$\hat{\Omega} = \frac{\Omega\,b}{2V_t}, \quad \hat{p}_{\text{osc}} = \frac{p_{\text{osc}}\,b}{2V_t}, \quad \hat{q}_{\text{osc}} = \frac{q_{\text{osc}}\,\bar{c}}{2V_t}, \quad \hat{r}_{\text{osc}} = \frac{r_{\text{osc}}\,b}{2V_t},$$

and the control surface angular deflections δ_e, δ_a, and δ_r.

Candidate regressors were composed of the explanatory variables in all polynomial combinations up to the third order. Transcendental functions and spline models of α and β were considered, but did not improve the results, likely because the aircraft remained within the post-stall aerodynamic regime throughout the spin. MOF modeling was used with analyst insight to study various model structures. Select results from MOF modeling for the nominal glide and steady spin maneuvers are displayed in Fig. 6, which shows the number of times each model term was selected for all the considered maneuvers. The candidate regressors are ordered based on the number of data sets for which the given regressor function made a significant contribution to model performance.

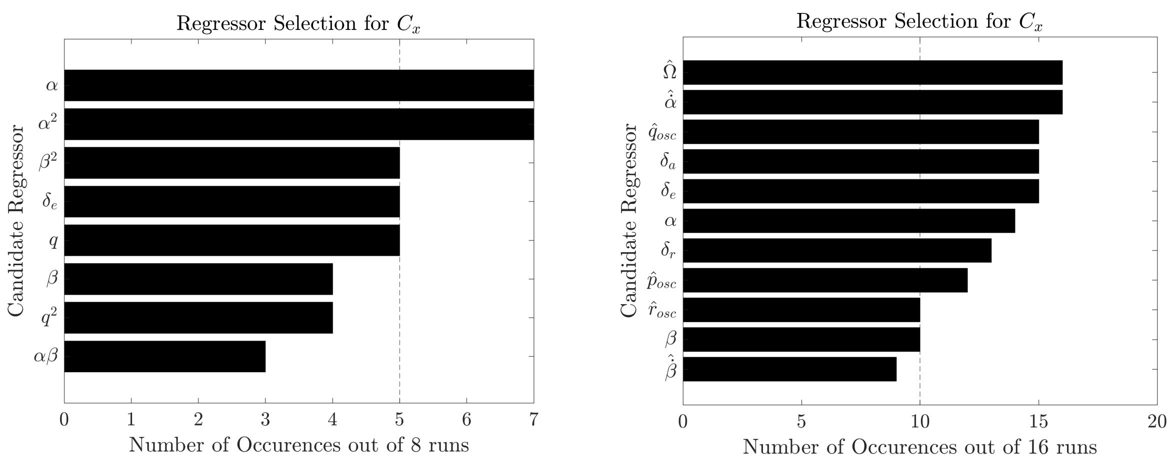

(a) Nominal glide **(b) Spin**

Fig. 6 Multivariate orthogonal function modeling select results.

For the nominal glide, the identified model structure for the force and moment coefficients is given in Eqs. (24)-(29). The model structure is valid in the normal operating range, including the onset of stall, but it does not capture post-stall effects or spin dynamics. For ease of comparison, regressors common to both the nominal glide and spin models are colored red.

$$C_x = C_{x_\alpha}\alpha + C_{x_q}\hat{q} + C_{x_{\delta_e}}\delta_e + C_{x_{(\alpha^2)}}(\alpha^2) + C_{x_{(\beta^2)}}(\beta^2) + C_{x_o} \tag{24}$$
$$C_y = C_{y_\beta}\beta + C_{y_p}\hat{p} + C_{y_r}\hat{r} + C_{y_{\delta_a}}\delta_a + C_{y_{\delta_r}}\delta_r + C_{y_o} \tag{25}$$
$$C_z = C_{z_\alpha}\alpha + C_{z_q}\hat{q} + C_{z_{\delta_e}}\delta_e + C_{z_{(\beta^2)}}(\beta^2) + C_{z_o} \tag{26}$$

$$C_l = C_{l_\beta}\beta + C_{l_p}\hat{p} + C_{l_r}\hat{r} + C_{l_{\delta_a}}\delta_a + C_{l_o} \tag{27}$$
$$C_m = C_{m_\alpha}\alpha + C_{m_q}\hat{q} + C_{m_{\delta_e}}\delta_e + C_{m_{(\alpha^2)}}(\alpha^2) + C_{m_{(\alpha^3)}}(\alpha^3) + C_{m_{(q^3)}}(\hat{q}^3) + C_{m_o} \tag{28}$$
$$C_n = C_{n_\beta}\beta + C_{n_p}\hat{p} + C_{n_r}\hat{r} + C_{n_{\delta_a}}\delta_a + C_{n_{\delta_r}}\delta_r + C_{n_{(\beta^2)}}(\beta^2) + C_{n_{(\beta^3)}}(\beta^3) + C_{n_o} \tag{29}$$

For the steady spins, the identified model structure for each force and moment coefficient is given in Eqs. (30)-(35).

$$\begin{aligned} C_x &= C_{x_\alpha}\alpha + C_{x_{\dot\alpha}}\hat{\dot\alpha} + C_{x_\beta}\beta + C_{x_\Omega}\hat\Omega + C_{x_{p_{osc}}}\hat p_{\text{osc}} + C_{x_{q_{osc}}}\hat q_{\text{osc}} + C_{x_{r_{osc}}}\hat r_{\text{osc}} \\ &\quad + C_{x_{\delta_e}}\delta_e + C_{x_{\delta_a}}\delta_a + C_{x_{\delta_r}}\delta_r + C_{x_{(\delta_e{}^2)}}(\delta_e{}^2) + C_{x_o} \end{aligned} \tag{30}$$

$$\begin{aligned} C_y &= C_{y_{\dot\alpha}}\hat{\dot\alpha} + C_{y_\beta}\beta + C_{y_{\dot\beta}}\hat{\dot\beta} + C_{y_\Omega}\hat\Omega + C_{y_{p_{osc}}}\hat p_{\text{osc}} + C_{y_{q_{osc}}}\hat q_{\text{osc}} + C_{y_{r_{osc}}}\hat r_{\text{osc}} \\ &\quad + C_{y_{\delta_e}}\delta_e + C_{y_{\delta_a}}\delta_a + C_{y_{\delta_r}}\delta_r + C_{y_{(\delta_e{}^2)}}(\delta_e{}^2) + C_{y_o} \end{aligned} \tag{31}$$

$$\begin{aligned} C_z &= C_{z_\alpha}\alpha + C_{z_{\dot\alpha}}\hat{\dot\alpha} + C_{z_\beta}\beta + C_{z_\Omega}\hat\Omega + C_{z_{p_{osc}}}\hat p_{\text{osc}} + C_{z_{q_{osc}}}\hat q_{\text{osc}} + C_{z_{r_{osc}}}\hat r_{\text{osc}} \\ &\quad + C_{z_{\delta_e}}\delta_e + C_{z_{\delta_a}}\delta_a + C_{z_{\delta_r}}\delta_r + C_{z_{(\delta_e{}^2)}}(\delta_e{}^2) + C_{z_{(\delta_e\delta_a)}}(\delta_e\delta_a) + C_{z_o} \end{aligned} \tag{32}$$

$$\begin{aligned} C_l &= C_{l_\alpha}\alpha + C_{l_{\dot\alpha}}\hat{\dot\alpha} + C_{l_\beta}\beta + C_{l_{\dot\beta}}\hat{\dot\beta} + C_{l_\Omega}\hat\Omega + C_{l_{p_{osc}}}\hat p_{\text{osc}} + C_{l_{q_{osc}}}\hat q_{\text{osc}} + C_{l_{r_{osc}}}\hat r_{\text{osc}} \\ &\quad + C_{l_{\delta_e}}\delta_e + C_{l_{\delta_a}}\delta_a + C_{l_{\delta_r}}\delta_r + C_{l_{(\delta_r{}^2)}}(\delta_r{}^2) + C_{l_o} \end{aligned} \tag{33}$$

$$\begin{aligned} C_m &= C_{m_\alpha}\alpha + C_{m_{\dot\alpha}}\hat{\dot\alpha} + C_{m_\beta}\beta + C_{m_\Omega}\hat\Omega + C_{m_{p_{osc}}}\hat p_{\text{osc}} + C_{m_{q_{osc}}}\hat q_{\text{osc}} + C_{m_{r_{osc}}}\hat r_{\text{osc}} \\ &\quad + C_{m_{\delta_e}}\delta_e + C_{m_{\delta_a}}\delta_a + C_{m_{\delta_r}}\delta_r + C_{m_{(\delta_e{}^2)}}(\delta_e{}^2) + C_{m_{(\delta_e\delta_a)}}(\delta_e\delta_a) + C_{m_o} \end{aligned} \tag{34}$$

$$\begin{aligned} C_n &= C_{n_\alpha}\alpha + C_{n_{\dot\alpha}}\hat{\dot\alpha} + C_{n_\beta}\beta + C_{n_{\dot\beta}}\hat{\dot\beta} + C_{n_\Omega}\hat\Omega + C_{n_{p_{osc}}}\hat p_{\text{osc}} + C_{n_{q_{osc}}}\hat q_{\text{osc}} + C_{n_{r_{osc}}}\hat r_{\text{osc}} \\ &\quad + C_{n_{\delta_e}}\delta_e + C_{n_{\delta_a}}\delta_a + C_{n_{\delta_r}}\delta_r + C_{n_{(\delta_a{}^2)}}(\delta_a{}^2) + C_{n_o} \end{aligned} \tag{35}$$

The model captures longitudinal and lateral-directional coupling, post-stall effects, and spin dynamics. The model structure is valid around a perturbation range centered at the nominal spin for 70% left rudder deflection, 70% trailing-edge up elevator, and 50% aileron deflection for left roll input.

C. Parameter Estimates

Parameter estimates were determined using ordinary least-squares regression (an equation error method) in the time domain to analyze the data from each run independently. The median value of the set of parameter estimates obtained from analyzing different maneuvers was taken as the final value to minimize the impact of possible outliers. The uncertainty of the final parameter estimates, σ, was determined using the scaled median absolute deviation (MAD) for the data set, following the justification given in Ref. [9]. This value of σ was used to determine a 95% confidence interval (i.e., with 95% CI = $\pm 2\sigma$) similar to Refs. [8, 9]. Individual run uncertainty accounting for colored residuals [34] generally showed agreement with the 95% confidence interval determined using the MAD for the full data set, thus showing good quantification of the uncertainty of the model. Final parameter estimates for the nominal glide and spin models are shown in Table 2 and Table 3, respectively.

D. Validation

Model validation aims to demonstrate that an adequate model was developed by testing predictive capability using data not used for model identification [25]. Validation seeks to determine if 1) the model agrees sufficiently well with observed data and 2) the model is adequate for the intended purpose [23]. For this effort, validation focused on the first issue by comparing the model predictions to flight data from maneuvers excited with an independent validation multisine. The second issue is of primary importance for the model's use, as outlined in [1] for this case, and is adequately addressed when the problem that motivated the modeling effort is successfully resolved. To answer the question "Is the model good enough?" two primary metrics were used. For quantitative analysis, similar to Refs. [8, 9, 35], Theil's inequality coefficient (TIC) and range-normalized root-mean-square error (NRMSE) were determined for each model relative to a validation maneuver. TIC is calculated from

$$\text{TIC}_i = \frac{\sqrt{\frac{1}{N}(\boldsymbol{z}_i - \boldsymbol{y}_i)^T(\boldsymbol{z}_i - \boldsymbol{y}_i)}}{\sqrt{\frac{1}{N}\boldsymbol{z}_i^T\boldsymbol{z}_i} + \sqrt{\frac{1}{N}\boldsymbol{y}_i^T\boldsymbol{y}_i}} \tag{36}$$

where $\boldsymbol{z}_i$ is the ith force or moment coefficient ($i \in \{x, y, z, l, m, n\}$) calculated from measured flight data and $\boldsymbol{y}_i$ is the model predicted ith force or moment coefficient. TIC values range from 0 to 1, with a TIC value of 0 indicating a perfect

Table 2 Nominal glide model

	$\hat{\theta} \pm \sigma$
C_{x_α}	+0.275 ± 0.089
C_{x_q}	+2.146 ± 1.661
$C_{x_{\delta e}}$	+0.170 ± 0.051
$C_{x_{(\alpha^2)}}$	+2.529 ± 0.607
$C_{x_{(\beta^2)}}$	+0.233 ± 0.105
C_{x_o}	-0.075 ± 0.004
C_{y_β}	-0.570 ± 0.022
C_{y_p}	-0.501 ± 0.049
C_{y_r}	+0.402 ± 0.050
$C_{y_{\delta a}}$	-0.362 ± 0.026
$C_{y_{\delta r}}$	+0.118 ± 0.007
C_{y_o}	+0.006 ± 0.012
C_{z_α}	-4.260 ± 0.415
C_{z_q}	-8.902 ± 5.056
$C_{z_{\delta e}}$	-0.617 ± 0.118
$C_{z_{(\beta^2)}}$	-0.538 ± 0.467
C_{z_o}	-0.297 ± 0.029
C_{l_β}	-0.084 ± 0.008
C_{l_p}	-0.600 ± 0.035
C_{l_r}	+0.134 ± 0.016
$C_{l_{\delta a}}$	-0.370 ± 0.011
C_{l_o}	-0.002 ± 0.005
C_{m_α}	-0.584 ± 0.053
C_{m_q}	-9.137 ± 1.275
$C_{m_{\delta e}}$	-0.764 ± 0.053
$C_{m_{(\alpha^2)}}$	-1.636 ± 0.480
$C_{m_{(\alpha^3)}}$	-3.116 ± 5.172
$C_{m_{(q^3)}}$	-0.132 ± 0.000
C_{m_o}	+0.012 ± 0.003
C_{n_β}	+0.056 ± 0.003
C_{n_p}	+0.043 ± 0.007
C_{n_r}	-0.118 ± 0.011
$C_{n_{\delta a}}$	+0.074 ± 0.012
$C_{n_{\delta r}}$	-0.046 ± 0.001
$C_{n_{(\beta^2)}}$	+0.025 ± 0.030
$C_{n_{(\beta^3)}}$	+0.239 ± 0.107
C_{n_o}	+0.003 ± 0.002

Table 3 Spin model

	$\hat{\theta} \pm \sigma$		$\hat{\theta} \pm \sigma$
C_{x_α}	+0.059 ± 0.032	C_{l_α}	-0.022 ± 0.026
$C_{x_{\dot\alpha}}$	-4.801 ± 0.886	$C_{l_{\dot\alpha}}$	+4.509 ± 1.034
C_{x_β}	-0.005 ± 0.057	C_{l_β}	-0.060 ± 0.021
C_{x_Ω}	+0.402 ± 0.033	$C_{l_{\dot\beta}}$	+0.218 ± 0.111
$C_{x_{posc}}$	+0.019 ± 0.362	C_{l_Ω}	-0.077 ± 0.031
$C_{x_{qosc}}$	+5.148 ± 1.292	$C_{l_{posc}}$	+0.003 ± 0.186
$C_{x_{rosc}}$	-0.093 ± 0.123	$C_{l_{qosc}}$	-3.649 ± 1.136
$C_{x_{\delta e}}$	+0.090 ± 0.030	$C_{l_{rosc}}$	+0.323 ± 0.188
$C_{x_{\delta a}}$	-0.043 ± 0.023	$C_{l_{\delta e}}$	+0.029 ± 0.012
$C_{x_{\delta r}}$	-0.033 ± 0.009	$C_{l_{\delta a}}$	-0.093 ± 0.023
$C_{x_{(\delta e^2)}}$	+0.241 ± 0.215	$C_{l_{\delta r}}$	-0.020 ± 0.026
C_{x_o}	-0.125 ± 0.013	$C_{l_{(\delta r^2)}}$	+0.214 ± 0.099
$C_{y_{\dot\alpha}}$	+14.196 ± 2.365	C_{l_o}	+0.007 ± 0.003
C_{y_β}	-0.462 ± 0.063	C_{m_α}	-0.150 ± 0.169
$C_{y_{\dot\beta}}$	+0.913 ± 0.310	$C_{m_{\dot\alpha}}$	+18.456 ± 8.733
C_{y_Ω}	+0.028 ± 0.076	C_{m_β}	-0.049 ± 0.234
$C_{y_{posc}}$	+0.027 ± 0.239	C_{m_Ω}	+0.107 ± 0.234
$C_{y_{qosc}}$	-7.796 ± 1.994	$C_{m_{posc}}$	+0.523 ± 0.747
$C_{y_{rosc}}$	+1.020 ± 0.333	$C_{m_{qosc}}$	-19.230 ± 8.023
$C_{y_{\delta e}}$	-0.093 ± 0.059	$C_{m_{rosc}}$	+0.391 ± 0.679
$C_{y_{\delta a}}$	-0.012 ± 0.057	$C_{m_{\delta e}}$	-0.159 ± 0.076
$C_{y_{\delta r}}$	+0.069 ± 0.025	$C_{m_{\delta a}}$	+0.025 ± 0.126
$C_{y_{(\delta e^2)}}$	-0.878 ± 0.461	$C_{m_{\delta r}}$	-0.052 ± 0.069
C_{y_o}	-0.064 ± 0.015	$C_{m_{(\delta e^2)}}$	-0.781 ± 0.612
C_{z_α}	-0.177 ± 0.391	$C_{m_{(\delta e\,\delta a)}}$	-0.470 ± 0.370
$C_{z_{\dot\alpha}}$	+66.100 ± 23.248	C_{m_o}	+0.004 ± 0.016
C_{z_β}	-0.244 ± 0.163	C_{n_α}	+0.048 ± 0.012
C_{z_Ω}	+0.252 ± 0.264	$C_{n_{\dot\alpha}}$	-0.764 ± 0.237
$C_{z_{posc}}$	+2.055 ± 1.379	C_{n_β}	+0.020 ± 0.011
$C_{z_{qosc}}$	-60.155 ± 22.772	$C_{n_{\dot\beta}}$	-0.055 ± 0.057
$C_{z_{rosc}}$	+0.997 ± 0.971	C_{n_Ω}	+0.033 ± 0.014
$C_{z_{\delta e}}$	+0.130 ± 0.210	$C_{n_{posc}}$	+0.073 ± 0.054
$C_{z_{\delta a}}$	+0.052 ± 0.211	$C_{n_{qosc}}$	+0.581 ± 0.233
$C_{z_{\delta r}}$	-0.054 ± 0.100	$C_{n_{rosc}}$	-0.201 ± 0.052
$C_{z_{(\delta e^2)}}$	-1.925 ± 2.058	$C_{n_{\delta e}}$	-0.002 ± 0.003
$C_{z_{(\delta e\,\delta a)}}$	-0.655 ± 1.150	$C_{n_{\delta a}}$	+0.039 ± 0.012
C_{z_o}	-0.859 ± 0.098	$C_{n_{\delta r}}$	-0.041 ± 0.006
		$C_{n_{(\delta a^2)}}$	-0.056 ± 0.066
		C_{n_o}	+0.001 ± 0.002

model fit. A TIC value below 0.3 is considered good agreement between validation data and model predictions [25]. Similarly, NRMSE is calculated for each force and moment coefficient from

$$\text{NRMSE}_i = 100 \times \frac{1}{\text{range}(z_i)} \sqrt{\frac{(z_i - y_i)^T (z_i - y_i)}{N}} \tag{37}$$

A NRMSE value of 0 indicates a perfect model fit and the magnitude can be interpreted similar to a percent error. Range normalization provides a fair assessment of the error for coefficients such as C_x and C_z which are not centered about zero [35].

The nonlinear model predictions for each flight condition (nominal glide and spin) were validated against flight data from maneuvers excited with an independent validation multisine which was developed with a different power spectral density than the one used for modeling. This "acid test," as described in Ref. [25], duly challenges the model by using data that were not included in the modeling process and were obtained using a different excitation. Three validation cases are considered here for comparison:

1) The nominal glide model is validated against an independent multisine maneuver in a nominal glide.
2) The nominal glide model is validated against an independent multisine spin maneuver.
3) The spin model is validated against an independent multisine spin maneuver.

For the nominal glide maneuver, quantitative validation results are shown in Table 4. For the spin maneuver, quantitative validation results are shown in Table 5. Figures 7 and 8 show the validation results for a nominal glide maneuver and a spin maneuver with the independent multisine, along with the smoothed flight data. The same flight data are used for both the nominal glide model and spin model validation to directly compare model performance in a spin.

Table 4 Nominal glide maneuver validation metrics

Model basis	C_x	C_y	C_z	C_l	C_m	C_n
Theil's inequality coefficient (TIC) - 0 indicates perfect model fit						
Nominal glide	0.0859	0.0864	0.1024	0.2273	0.2350	0.1027
Normalized root-mean-square error (NRMSE) - 0 indicates perfect model fit						
Nominal glide	8.3737	4.6227	9.2919	8.4009	9.5217	4.4939

Table 5 Spin maneuver model validation metrics

Model basis	C_x	C_y	C_z	C_l	C_m	C_n
Theil's inequality coefficient (TIC) - 0 indicates perfect model fit						
Nominal glide	0.3159	0.3235	0.1525	0.7089	0.7875	0.5495
Spin	0.0267	0.1180	0.0158	0.3671	0.3924	0.3139
Normalized root-mean-square error (NRMSE) - 0 indicates perfect model fit						
Nominal glide	99.0666	37.0473	64.1838	45.9437	84.1530	37.8778
Spin	7.8525	12.3143	6.5053	12.7085	13.3728	15.3302

For the nominal glide model validated against a nominal glide maneuver the TIC values are reasonably close to 0, indicating a good fit for the data. Additionally, the relatively low NRMSE values demonstrate adequate model performance. For the spin model validated against a spin maneuver, the low TIC and NRMSE values also indicate adequate model performance. Visual inspection of nominal glide model predictions to nominal glide validation data (Fig. 7) and spin model predictions to spin validation data (Fig. 8b) shows good matching between flight data and the model predicted force and moment coefficients.

On the contrary, the nominal glide model does not validate well against the spin maneuver. Relatively high TIC and NRMSE values indicate poor model performance. Visual inspection of the model predicted force and moment coefficients in Fig. 8a shows the nominal glide model predicts exaggerated aircraft response while the aircraft is in a spin. This indicates the nominal glide model is not a good predictor of spin dynamics.

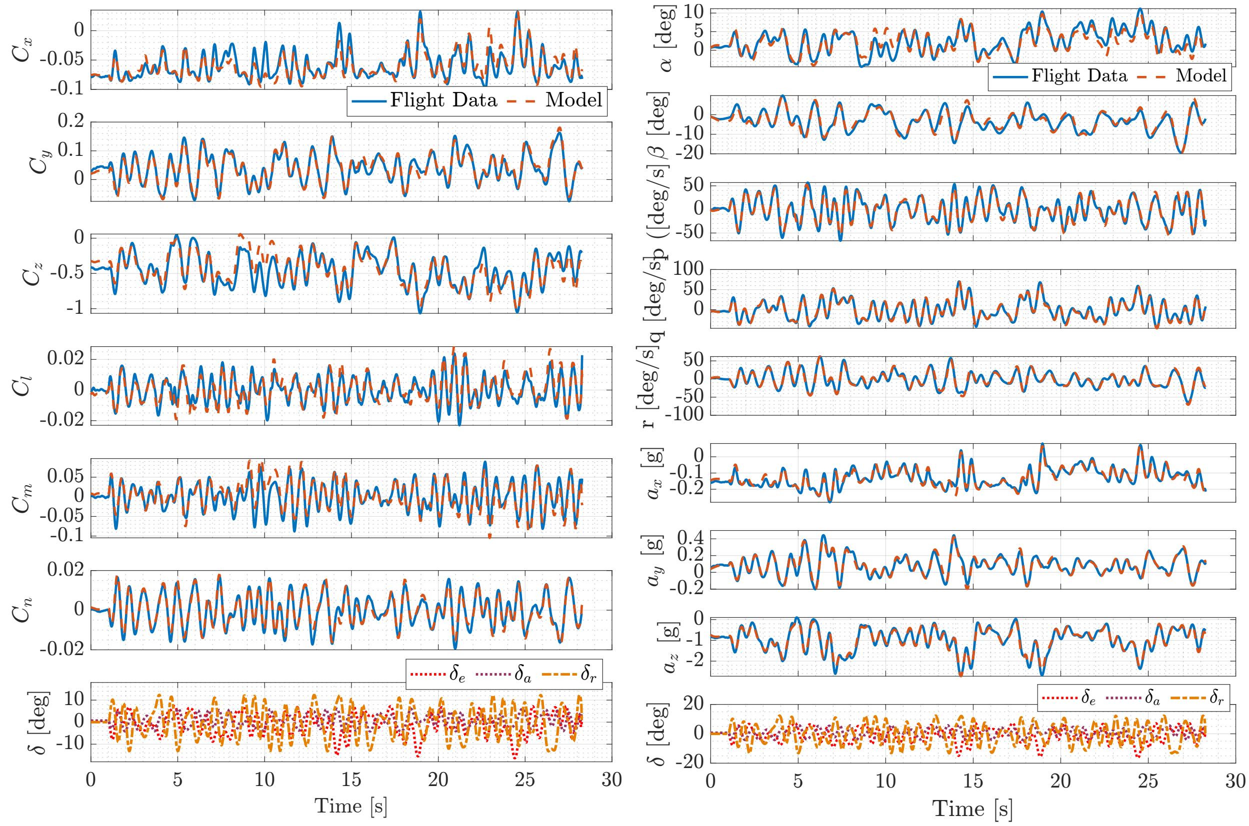

(a) Force and moment coefficient prediction

(b) Output prediction

Fig. 7 Validation results for nominal glide model for nominal glide maneuver with multisine inputs.

V. Conclusion

In the investigation described here, a nonlinear, coupled aerodynamic model was developed for a fixed-wing aircraft in a nominal glide as well as a nonlinear, quasi-steady, coupled aerodynamic model for spinning descent. New methods were proposed to adequately describe the aircraft dynamics and control authority in the neighborhood of a stable, oscillatory spin. To the best of the authors' knowledge, orthogonal phase-optimized multisine inputs were used for the first time as excitation signals while collecting spinning flight data and a new decomposition of explanatory variables led to an elegant model structure for spin flight data analysis. The results show that the nominal glide flight dynamic model predictions match validation data well for conventional flight, though not for spinning descent. Predictions using the model developed for spinning flight, on the other hand, do adequately match validation data for a stable, oscillatory, spinning descent.

Intuitively, a model-based control law that is developed using the more accurate spinning flight model would perform better than one developed using the nominal glide flight model. As illustrated here, however, developing a spinning flight model is not a trivial exercise due to the nonlinear, unsteady, and coupled aerodynamics. One question being addressed in ongoing research is whether an effective robust control law can be designed using a nominal envelope flight dynamic model. If not, then a spinning flight model might be required to design a controller that can direct the flight path of an aircraft in a terminal spin. In any case, the spinning flight model can be used to assess and tune performance in advance of flight tests involving closed-loop control.

Acknowledgments

The authors thank Jean-Michel Fahmi and Mekonen Halefom for flight test experiment support. We also gratefully acknowledge financial support from the United States Air Force Test Pilot School under USAF Contract No. FA9302-18-P-5227 and from NASA under Grant No. 80NSSC20M0162. The first author is grateful to the United States Air Force and the Dominion Energy Research Fellowship at Virginia Tech for financial support.

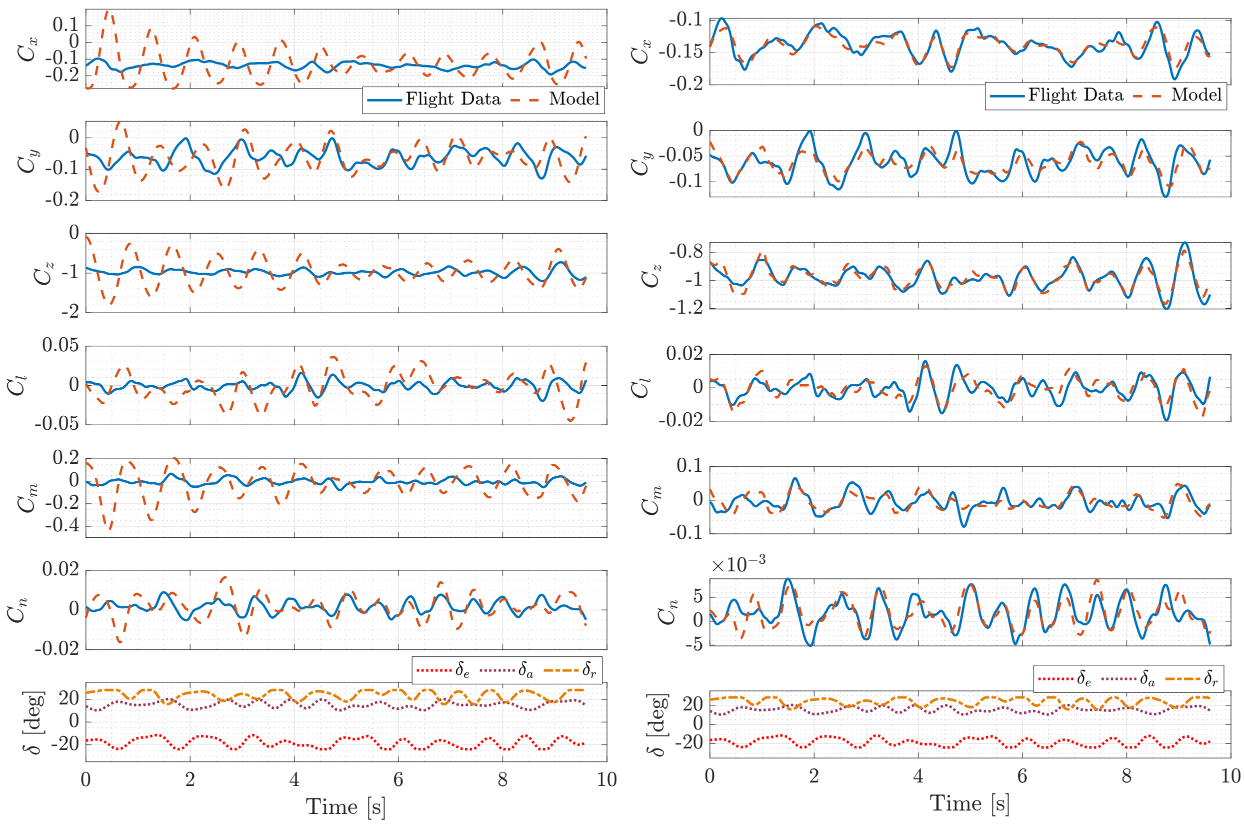

(a) Nominal glide model

(b) Spin model

Fig. 8 Comparison of validation results for a spin maneuver with multisine inputs (same spin flight data).

References

[1] Hopwood, J. W., Gresham, J. L., and Woolsey, C. A., "Stall Spin Flight Path Control Using Parallel Yaw-Periodic Linear Quadratic and Robust H_∞ Controllers," *AIAA SciTech 2022 Forum*, 2022, pp. 1–15. To be published.

[2] Morelli, E. A., and Klein, V., *Aircraft System Identification: Theory and Practice*, 2$^{\text{nd}}$ ed., Sunflyte Enterprises, Williamsburg, VA, 2016.

[3] Morelli, E. A., "Multiple Input Design for Real-Time Parameter Estimation in the Frequency Domain," *13th IFAC Conference on System Identification*, 2003, pp. 1–6. https://doi.org/10.1016/S1474-6670(17)34833-4.

[4] Kinzig, B., "Global Hawk Systems Engineering Case Study," Tech. rep., Air Force Institute of Technology, Fort Belvoir, VA, Jan. 2010. https://doi.org/10.21236/ADA538761.

[5] Stansbury, R. S., Tanis, W., and Wilson, T. A., "A Technology Survey of Emergency Recovery and Flight Termination Systems for UAS," *AIAA Infotech*, AIAA Paper 2009-2038, 2009, pp. 1–8. https://doi.org/10.2514/6.2009-2038.

[6] Carney, E., Castano, L., and Xu, H., "Determination of Safe Landing Zones for an Autonomous UAS Using Elevation and Population Density Data," *AIAA SciTech Forum*, AIAA Paper 2019-1060, 2019, pp. 1–16. https://doi.org/10.2514/6.2019-1060.

[7] Shukla, P., and Woolsey, C. A., "Active Flight Path Control for an Induced Spin Flight Termination System," *2018 AIAA Atmospheric Flight Mechanics Conference*, AIAA Paper 2018-0528, 2018, pp. 1–18. https://doi.org/10.2514/6.2018-0528.

[8] Gresham, J. L., Simmons, B. M., Fahmi, J.-M. W., and Woolsey, C. A., "Remote Uncorrelated Pilot Inputs for Nonlinear Aerodynamic Model Identification from Flight Data," *AIAA AVIATION 2021 FORUM*, AIAA Paper 2021-2792, 2021, pp. 1–26. https://doi.org/10.2514/6.2021-2792.

[9] Simmons, B. M., McClelland, H. G., and Woolsey, C. A., "Nonlinear Model Identification Methodology for Small, Fixed-Wing, Unmanned Aircraft," *Journal of Aircraft*, Vol. 56, No. 3, 2019, pp. 1056–1067. https://doi.org/10.2514/1.C035160.

[10] Gresham, J. L., Fahmi, J.-M., Simmons, B. M., Hopwood, J. W., Foster, J. W., and Woolsey, C. A., "Flight Test Approach for Modeling and Control Law Validation for Unmanned Aircraft," *AIAA SciTech 2022 Forum*, 2022, pp. 1–16. To be published.

[11] Tischler, M. B., and Barlow, J. B., "Determination of the Spin and Recovery Characteristics of a General Aviation Design," *Journal of Aircraft*, Vol. 18, No. 4, 1981, pp. 238–244. https://doi.org/10.2514/3.57487.

[12] Bihrle, W., and Barnhart, B., "Spin Prediction Techniques," *Journal of Aircraft*, Vol. 20, No. 2, 1983, pp. 97–101. https://doi.org/10.2514/3.44837.

[13] Murch, A., and Foster, J., "Recent NASA Research on Aerodynamic Modeling of Post-Stall and Spin Dynamics of Large Transport Airplanes," *45th AIAA Aerospace Sciences Meeting and Exhibit*, AIAA Paper 2007-463, 2007, pp. 1–20. https://doi.org/10.2514/6.2007-463.

[14] Farcy, D., Khrabrov, A. N., and Sidoryuk, M. E., "Sensitivity of Spin Parameters to Uncertainties of the Aircraft Aerodynamic Model," *Journal of Aircraft*, Vol. 57, No. 5, 2020, pp. 922–937. https://doi.org/10.2514/1.C035882.

[15] Craig, A., and Romani, D., Jr., "Unsteady Aerodynamics in Airplane Stall-Spin Departure," *31st Aerospace Sciences Meeting*, AIAA Paper 1993-622, 1993, pp. 1–7. https://doi.org/10.2514/6.1993-622.

[16] Owens, B., Brandon, J., Croom, M., Fremaux, M., Heim, G., and Vicroy, D., "Overview of Dynamic Test Techniques for Flight Dynamics Research at NASA LaRC," *25th AIAA Aerodynamic Measurement Technology and Ground Testing Conference*, AIAA Paper 2006-3146, 2006, pp. 1–22. https://doi.org/10.2514/6.2006-3146.

[17] Kathy Barnstorff, "NASA Langley Puts Research into a Spin for 75 Years," , March 2016. URL https://www.nasa.gov/feature/langley/nasa-langley-puts-research-into-a-spin-for-75-years.

[18] Dias, J. N., "Identification of High Angle of Attack Aerodynamic Model Using Flight Data from Spin Tests," *2013 SFTE 44th Annual International Symposium*, Society of Flight Test Engineers, 2013, pp. 1–26.

[19] Mokhtari, M., and Sabzehparvar, M., "Identification of Spin Maneuver Aerodynamic Nonlinear Model by Applying Ensemble Empirical Mode Decomposition and Extended Multipoint Modeling," *Proceedings of the Institution of Mechanical Engineers, Part G: Journal of Aerospace Engineering*, Vol. 233, No. 5, 2019, pp. 1865–1878. https://doi.org/10.1177/0954410018764937.

[20] Brandt, S. A., Stiles, R. J., Bertin, J. J., and Whitford, R., *Introduction to Aeronautics: A Design Perspective*, 3rd ed., AIAA, Reston, VA, 2015.

[21] Martin, C., "The Spinning of Aircraft - A Discussion of Spin Prediction Techniques Including a Chronological Bibliography," Aerodynamics Report 177, Department of Defence, Defence Science and Technology Organisation Aeronautical Research Laboratory, Melbourne, Victoria, Australia, Aug. 1988.

[22] Tischler, M. B., and Barlow, J. B., "Dynamic Analysis of the Flat Spin Mode of a General Aviation Aircraft," *Journal of Aircraft*, Vol. 19, No. 3, 1982, pp. 198–205. https://doi.org/10.2514/3.57376.

[23] Ljung, L., *System Identification: Theory for the User*, 2nd ed., Prentice Hall PTR, Upper Saddle River, NJ, 1999.

[24] Morelli, E. A., "Global Nonlinear Aerodynamic Modeling Using Multivariate Orthogonal Functions," *Journal of Aircraft*, Vol. 32, No. 2, 1995, pp. 270–277. https://doi.org/10.2514/3.46712.

[25] Jategaonkar, R., *Flight Vehicle System Identification: A Time Domain Methodology*, 2nd ed., AIAA/Aerospace Press, Reston, VA, 2015. https://doi.org/10.2514/4.102790.

[26] Morelli, E., "Efficient Global Aerodynamic Modeling from Flight Data," *50th AIAA Aerospace Sciences Meeting including the New Horizons Forum and Aerospace Exposition*, AIAA Paper 2012-1050, 2012, pp. 1–21. https://doi.org/10.2514/6.2012-1050.

[27] "Cube Orange Flight Controller," https://docs.px4.io/master/en/flight_controller/cubepilot_cube_orange.html, Accessed May 2021.

[28] Miller, M. P., "An Accurate Method of Measuring the Moments of Inertia of Airplanes," *NACA Technical Note*, 1930.

[29] "Using the Estimation and Control Library Extended Kalman Filter," https://docs.px4.io/master/en/advanced_config/tuning_the_ecl_ekf.html, Accessed Feb 2021.

[30] Simmons, B. M., "System Identification of a Nonlinear Flight Dynamics Model for a Small, Fixed-Wing UAV," Master's thesis, Virginia Polytechnic Institute and State University (Virginia Tech), Blacksburg, VA, 2018.

[31] "Kentland Experimental Aerial Systems (KEAS) Laboratory," https://www.aoe.vt.edu/research/facilities/keas.html, Accessed Apr 2021.

[32] MATLAB, *MATLAB Documentation, version 9.9.0.1538559 (R2020b Update 3)*, The MathWorks Inc., Natick, Massachusetts, 2020.

[33] Morelli, E. A., "Real-Time Global Nonlinear Aerodynamic Modeling for Learn-To-Fly," *AIAA Atmospheric Flight Mechanics Conference*, AIAA Paper 2016-2010, 2016, pp. 1–22. https://doi.org/10.2514/6.2016-2010.

[34] Morelli, E. A., and Klein, V., "Accuracy of Aerodynamic Model Parameters Estimated from Flight Test Data," *Journal of Guidance, Control, and Dynamics*, Vol. 20, No. 1, 1997, pp. 74–80. https://doi.org/10.2514/2.3997.

[35] Simmons, B. M., "System Identification for Propellers at High Incidence Angles," *Journal of Aircraft*, Vol. 58, No. 6, 2021, pp. 1336–1350. https://doi.org/10.2514/1.C036329.